Draft version December 6, 2022
Typeset using LaTeX default style in AASTeX631

Calibrating Gamma-Ray Bursts by Using a Gaussian Process with Type Ia Supernovae

Nan Liang,[1,2,*] Zihao Li,[1,2,†] Xiaoyao Xie,[1,2,‡] and Puxun Wu[3,§]

[1] Key Laboratory of Information and Computing Science Guizhou Province, Guizhou Normal University, Guiyang, Guizhou 550025, China

[2] Joint Center for FAST Sciences Guizhou Normal University Node, Guiyang, Guizhou 550025, China

[3] Department of Physics and Synergistic Innovation Center for Quantum Effects and Applications, Hunan Normal University, Changsha, Hunan 410081, China

(Received; Revised; Accepted)

arXiv:2211.02473v2 [astro-ph.CO] 5 Dec 2022

ABSTRACT

In this paper, we calibrate the Amati relation (the $E_{\rm p}$-$E_{\rm iso}$ correlation) of gamma-ray bursts (GRBs) in a cosmology-independent way. By using Gaussian process to reconstruct the smoothed luminosity distance from the Pantheon type Ia supernovae (SNe Ia) sample, we utilize the reconstructed results to calibrate the $E_{\rm p}$-$E_{\rm iso}$ correlation with the Markov Chain Monte Carlo method and construct a Hubble diagram with the A220 GRB data, in which there are A118 GRB data with the higher qualities appropriate for cosmological purposes. With 98 GRBs at $1.4 < z \leq 8.2$ in the A118 sample and the observed Hubble data, we obtain $\Omega_{\rm m}$=$0.346^{+0.048}_{-0.069}$, h=$0.677^{+0.029}_{-0.029}$ for the flat ΛCDM model, and $\Omega_{\rm m}$=$0.314^{+0.072}_{-0.055}$, h=$0.705^{+0.055}_{-0.069}$, w=$-1.23^{+0.33}_{-0.64}$ for the flat wCDM model, which are consistent with those from fitting the coefficients of the Amati relation and the cosmological parameters simultaneously.

1. INTRODUCTION

Observations of type Ia supernovae (SNe Ia) provide a powerful probe in modern cosmology, from which the accelerated expansion of the universe has been found (Riess et al. 1998; Perlmutter et al. 1999). The maximum redshift observed by SNe Ia is about $z \sim 2.3$ (Scolnic et al. 2018). Thus, to explore the cosmic evolution at the high-redshift region requires observing more luminous objects than SNe Ia. Gamma-ray bursts (GRBs) are the strongest bursts of high-energy gamma rays from cosmological space in a short time, which are the most intense explosions observed so far. At present, the maximum redshift of the GRB can reach at $z = 9.4$ (Cucchiara et al. 2011). Therefore, GRBs can be used to probe the universe at the high redshift. Utilizing GRB in cosmology requires its luminosity relations, which are connections between measurable properties of the instantaneous gamma-ray emission and the luminosity or energy. Several empirical GRB luminosity relations have been proposed (Fenimore & Ramirez-Ruiz 2000; Norris et al. 2000; Amati et al. 2002; Ghirlanda et al. 2004a; Yonetoku et al. 2004; Liang & Zhang 2005; Firmani et al. 2006; Dainotti et al. 2008; Yu, Qi & Lu 2009; Tsutsui et al. 2009a; Izzo et al. 2015), see e.g., Ghirlanda et al. (2006), and Schaefer (2007) for reviews. According to these relations, the GRBs have been used as the cosmic probe for researching the evolving history of our universe and the properties of dark energy (Ghirlanda et al. 2004b; Dai et al. 2004; Firmani et al. 2005; Xu et al. 2005; Liang & Zhang 2006; Wang & Dai 2006; Schaefer 2007). For recent reviews of GRB luminosity relations and their applications in cosmology, see e.g. Wang et al. (2015), Dainotti & Del Vecchio (2017) and Dainotti & Amati (2018).

In the early cosmological research works of GRBs, a certain cosmological model was assumed to calibrate the GRB luminosity relation (Schaefer 2003; Dai et al. 2004; Schaefer 2007). When using these model-dependent GRB data to constrain the cosmological model, it suffers the so-called circularity problem (Ghirlanda et al. 2006). In order to avoid this circularity problem in the application of GRBs in cosmology, the simultaneous fitting method has been proposed (Amati et al. 2008; Li et al. 2008; Wang 2008), in which the coefficients of relations and the parameters of the cosmological model are constrained simultaneously. However, the circularity problem cannot be circumvented completely by means of statistical approaches, because a particular cosmological model is required in doing the joint fitting. Recently, Khadka & Ratra (2020) fitted simultaneously the cosmological and GRB relation

* liangn@bnu.edu.cn
† lizihao@gznu.edu.cn
‡ xyx@gznu.edu.cn
§ pxwu@hunnu.edu.cn

parameters in a number of different cosmological models, and found that the Amati relation parameters are almost identical in all cosmological models, which seems to indicate that these GRB data sets are standardizable within the error bars.

On the other hand, Liang et al. (2008) proposed a cosmological model-independent method to calibrate the luminosity relations of GRBs by using the SNe Ia data. It is obvious that objects at the same redshift should have the same luminosity distance in any cosmology. Therefore, in the same sense as using Cepheid variables to calibrate SNe Ia, if regarding SNe Ia as the first-order standard candles, GRBs can be calibrated from SNe Ia in a completely cosmological model-independent way. The luminosity distances at the redshift of the low-redshift GRB data can be derived by interpolating the SNe Ia data directly, and then the values of the coefficients of the GRB luminosity relation can be obtained from these low-redshift GRB data. Extrapolating these results on the high-redshift GRB data can build the GRB Hubble diagram. Thus, the standard Hubble diagram method can be used to constrain the cosmological model (Capozziello & Izzo 2008, 2009; Izzo et al. 2009; Wei & Zhang 2009; Wei 2010; Liang et al. 2010, 2011; Freitas et al. 2011; Wang et al. 2011; Wei 2015; Wang et al. 2016). Similar to the interpolation method, GRBs are calibrated from the SNe Ia by using the polynomial fitting (Kodama et al. 2008; Tsutsui et al. 2009b), an iterative procedure (Liang & Zhang 2008), the local regression (Cardone et al. 2009, 2011; Demianski & Piedipalumbo 2011; Demianski et al. 2011, 2017a), the cosmography methods [1](Capozziello & Izzo 2010; Wang & Dai 2011; Gao et al. 2012; Wang & Wang 2014), a two-steps method minimizing the use of SNe Ia (Izzo et al. 2015; Muccino et al. 2021), and the Padé approximation method (Liu & Wei 2015).

A Gaussian process is a fully Bayesian approach for smoothing data, which can effectively reduce the errors of reconstructed results compared to the approaches mentioned in the above. In recent years, a Gaussian process method has been widely applied to the field of cosmology and astrophysics (Seikel et al. 2012a,b; Busti et al. 2014; Yu & Wang 2016; Yu et al. 2018; Lin et al. 2018; Wei 2018; Pan et al. 2020; Sun et al. 2021; Avila et al. 2022). For examples, Seikel et al. (2012a) used a Gaussian process to reconstruct the luminosity distance with its derivatives and the dark energy dynamics from SNe Ia. Lin et al. (2018) constrained the distance duality relation with the Gaussian process from SNe Ia, galaxy clusters, and baryon acoustic oscillations. Sun et al. (2021) investigated the influence of the bounds of the hyperparameters on the reconstruction of the Hubble constant with the Gaussian process.

The Amati relation (Amati et al. 2002), which connects the spectral peak energy and the isotropic equivalent radiated energy (the $E_{\rm p}$-$E_{\rm iso}$ correlation) of GRBs, has been widely used in GRB cosmology (Amati et al. 2008; Wei & Zhang 2009; Demianski & Piedipalumbo 2011; Demianski et al. 2011, 2017a,b; Liu & Wei 2015; Feng & Li 2016). Wei (2010) calibrated 109 GRBs with the Amati relation, using the cosmology-independent calibration method proposed by Liang et al. (2008).Wang et al. (2016) used two model-independent methods to standardize the Amati relation with 151 GRB data (including the update 42 GRBs). Recently, Amati et al. (2019) proposed another similar cosmological model-independent method to calibrate the Amati relation by using the observed Hubble data (OHD) through the Bézier polynomial, and built up a new data set consisting of 193 GRBs (with firmly measured redshift and spectral parameters taken from Demianski et al. (2017a) and references therein). Fana Dirirsa et al. (2019) found that the Amati relation is satisfied by the 25 Fermi GRB sample. For comparisons, the authors also use a sample of 94 GRBs selected from 151 GRBs analyzed by Wang et al. (2016). For recent works that used the Amati relation for the application in cosmology, see, e.g. Wang & Wang (2019); Khadka & Ratra (2020); Shirokov et al. (2020); Demianski et al. (2021); Montiel et al. (2021); Tang et al. (2021); Luongo & Muccino (2021a,b); Khadka et al. (2021); Cao et al. (2021); Cao & Ratra (2022); Gowri & Shantanu (2022); Jia et al. (2022), and Muccino, Luongo & Jain (2022).

More recently, Khadka et al. (2021) used the Amati relation and the Combo-correlated GRB data sets[2] to simultaneously derive the correlation and cosmological model parameter constraints. For the Amati relation, the authors compile a data set of 118 bursts (the A118 sample), including recent Fermi observations samples from the total 220 GRBs (the A220 sample) with the smallest intrinsic dispersion, which is suitable for constraining cosmological parameters. With the A220 and the A118 GRB samples, Cao et al. (2022a,b) have used the Amati relation in conjunction with the Dainotti-correlated GRB data sets[3] compiled recently by Hu et al. (2021) and

[1] Model-independent techniques to calibrate GRB correlations have been investigated in the field of cosmography (see, e.g. Luongo & Muccino (2020)). The results look similar to those here presented, which are reasonable and interesting. Moreover, the cosmographic technique has been wildly used by several approaches in pure cosmology to investigate the expansion history of the universe (see, e.g. Aviles et al. (2012); Gruber & Luongo (2014); Dunsby & Luongo (2016); Capozziello, D'Agostino, & Luongo (2018)).

[2] The Combo relation (Izzo et al. 2015) is an hybrid correlation involving prompt and afterglow GRB parameters (i.e., the plateau luminosity L_0, the rest-frame duration τ, and the late power-law decay index α) with a small data scatter, which has been investigated by Muccino et al. (2021); Luongo & Muccino (2021a) and Tang et al. (2022).

[3] The Dainotti relation (Dainotti et al. 2008) between the plateau luminosity (L_0) and the end time of the plateau in X-ray afterglows (t_b) have been used for cosmological purposes (Hu et al. 2021; Wang et al. 2022; Cao et al. 2022a,b; Dainotti et al. 2022a,b,c). The similar relations with the plateau in the X-ray afterglows have been used in Xu et al. (2021).

Wang et al. (2022) to constrain cosmological model parameters; Liu et al. (2022a,b) have proposed the improved Amati relations, which contains a redshift-dependent term, via a powerful statistical tool called copula.

In this paper, we plan to use the Gaussian process to reconstruct the luminosity distance from the Pantheon SNe Ia sample (Scolnic et al. 2018), without assuming any specific form of the distance-redshift relation of SNe Ia, and then calibrate the Amati relation with the total 220 GRB samples and the A118 sample (Khadka et al. 2021) to obtain the GRB Hubble diagram at the high redshift. With 98 GRB data at $1.4 < z \leq 8.2$ in the A118 sample and the OHD, we constrain the ΛCDM model and wCDM model in flat space. Finally, we also use GRB data sets to constrain the cosmological models and GRB relation parameters simultaneously.

2. GRB HUBBLE DIAGRAM FROM LOW-REDSHIFT CALIBRATION

2.1. *GRBs calibration with the Amati relation at $z < 1.4$*

The Gaussian process can reconstruct effectively a smooth function from the discrete data points without assuming explicit fitting forms of the function. In the Gaussian process, the reconstructed function is a Gaussian random variable at a reconstructed point, which is completely confirmed by its mean function and covariance function. The function values $f(z)$ are correlated by a covariance function $k(z, \tilde{z})$ to characterize the connection between the function values at different reconstructed points (Seikel et al. 2012a). There are a lot of covariance functions available that we can choose. The advantage of the squared exponential covariance function is that it is infinitely differentiable, which is useful for reconstructing the derivative of a function (Seikel et al. 2012a). The squared exponential covariance function is given by

$$k(z, \tilde{z}) = \sigma_f^2 \exp\left[-\frac{(z-\tilde{z})^2}{2l^2}\right]. \tag{1}$$

The hyperparameter σ_f, which determines the typical change of $f(z)$, and l, which determines the length in the z-direction, can be optimized by maximizing the marginal likelihood.

We use public python package `GaPP`[4] to calibrate the GRB relation from the SNe Ia. For the GRB data set, we use the total 220 GRB data (A220)[5] including the recent Fermi observations (Khadka et al. 2021), as well as the higher-quality 118 data set (A118)[6] with a tighter intrinsic scatter. For SNe Ia data sets, we use the Pantheon sample (Scolnic et al. 2018), which contained 1048 SNe Ia data points with the apparent magnitude. The distance modulus relates to the luminosity distance d_L through $\mu = m - M = 5\log_{10}(\frac{d_L}{\mathrm{Mpc}}) + 25$, where m and M are the apparent magnitude and the absolute magnitude, respectively. In this procedure, we reconstruct the apparent magnitude of GRBs from SNe Ia. The apparent magnitudes reconstructed from the Gaussian process with the 1σ uncertainty from SNe Ia data are plotted in Figure 1.

We find that the reconstructed function presents strange oscillations with a large uncertainty in the range where data points are sparse at $1.4 \leq z \leq 2.3$. Thus, the lack of SNe Ia at $z \geq 1.4$ in the `GaPP` procedure will produce the limits of Gaussian processes, which may affect the overall analysis of data comparisons. However, after removing SNe Ia data at $1.4 \leq z \leq 2.3$, we find that the apparent magnitudes reconstructed from SNe Ia data at $z < 1.4$ are almost identical with those reconstructed from SNe Ia data at $z \leq 2.3$. This indicates that this limitation does not affect the reconstructed results in the redshift region $z < 1.4$, which can be seen in Figure 1. Therefore we can use the luminosity distance reconstructing from SNe Ia at $z < 2.3$ to calibrate the Amati relation with 79 GRBs of A220 and 20 GRBs of A118 at $z < 1.4$.

The Amati relation can be expressed as

$$y = a + bx, \tag{2}$$

where $y = \log_{10}\frac{E_{\mathrm{iso}}}{1\mathrm{erg}}$, $x = \log_{10}\frac{E_{\mathrm{p}}}{300\mathrm{keV}}$, E_{p} and E_{iso} are the spectral peak energy and the isotropic equivalent radiated energy, and a and b are free coefficients needing to be calibrated from the observed data. E_{iso} and E_{p} can be calculated through

$$E_{\mathrm{iso}} = 4\pi d_L^2(z) S_{\mathrm{bolo}}(1+z)^{-1}, \quad E_{\mathrm{p}} = E_{\mathrm{p}}^{\mathrm{obs}}(1+z), \tag{3}$$

where $E_{\mathrm{p}}^{\mathrm{obs}}$ and S_{bolo} are the GRB spectral peak energy and bolometric fluence, which are the observables.

[4] https://github.com/astrobengaly/GaPP

[5] The A220 data set is composed of 220 long GRBs (Khadka et al. 2021), including A118 data sets, as well as 102 data sets (A102) from 193 GRBs analyzed by Amati et al. (2019) and Demianski et al. (2017a), which have not already been included in the A118 sample.

[6] The A118 data set is composed of 118 long GRBs (Khadka et al. 2021), including 25 long GRBs with Fermi-GBM/LAT data and well-constrained spectral properties (Fana Dirirsa et al. 2019), as well as 93 bursts updated from a sample of 94 GRBs (with GRB 020127 removed because its redshift is not secure) selected from 151 GRBs analyzed by Wang et al. (2016).

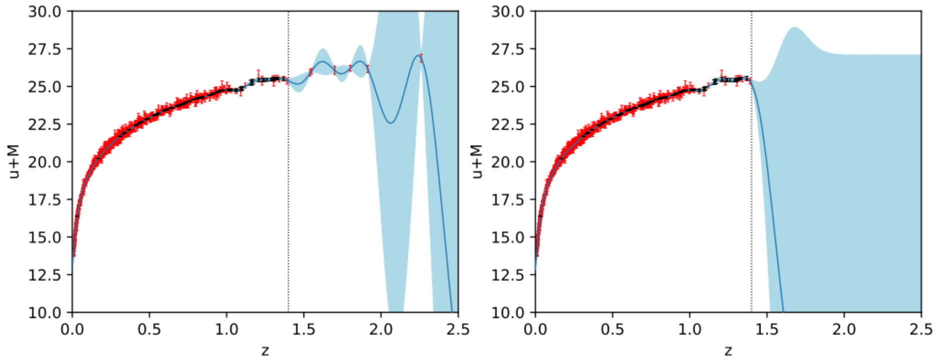

Figure 1. The apparent magnitudes reconstructed through the Gaussian process from SNe Ia data at $z \leq 2.3$ (left panel), and those reconstructed from SNe Ia data at $z < 1.4$ (right panel). The blue curves present the reconstructed function with the 1σ uncertainty from the SNe Ia data (red dots). The apparent magnitudes of GRBs at $z < 1.4$ (black dots) are reconstructed from SNe Ia through the Gaussian process. The dashed line denotes $z = 1.4$.

We determine the parameters of the Amati relation from the GRB sample at $z < 1.4$, which are shown in Figure. 1, by using the method of the likelihood function (D'Agostini 2005)

$$\mathcal{L}(\sigma, a, b, M) \propto \prod_{i=1}^{N_1} \frac{1}{\sigma^2} \times \exp\left[-\frac{[y_i - y(x_i, z_i; a, b, M)]^2}{2\sigma^2}\right]. \tag{4}$$

Here $N_1 = 79$ or 20 denotes the number of low-redshift GRBs in A220 or A118 data sets, $\sigma = \sqrt{\sigma_{\rm int}^2 + \sigma_{y,i}^2 + b^2\sigma_{x,i}^2}$, $\sigma_{\rm int}$ is the intrinsic scatter of GRBs, $\sigma_y = \frac{1}{\ln 10}\frac{\sigma_{E_{\rm iso}}}{E_{\rm iso}}$, $\sigma_x = \frac{1}{\ln 10}\frac{\sigma_{E_{\rm p}}}{E_{\rm p}}$, $\sigma_{E_{\rm p}}$ is the error magnitude of the spectral peak energy, and $\sigma_{E_{\rm iso}} = 4\pi d_L^2 \sigma_{S_{\rm bolo}}(1+z)^{-1}$ is the error magnitude of isotropic equivalent radiated energy, where $\sigma_{S_{\rm bolo}}$ is the error magnitude of bolometric fluence.

We use the python package `emcee` (Foreman-Mackey et al. 2013), which is optimized on the basis of the Metropolis-Hastings algorithm, to implement Markov Chain Monte Carlo (MCMC) numerical fitting method. The absolute magnitude M of SNe Ia should be fitted simultaneously with the calibration parameters a and b.[7] The number of points that have been used in each *emcee* procedure is 8000. The calibrated results are summarized in Table 1, and plotted in Figure 2. We find that the values of absolute magnitude with the A220 GRB data set and the A118 GRB data set are almost the same ($M = -19.50^{+1.40}_{-1.40}$). The results of the intercept a with the A220 GRB data set are well consistent at 1σ with the A118 GRB data set, while the difference of the slope b between A220 and A118 is very significant. Moreover, the value of the 1σ uncertainty of the slope b in A220 is smaller than that in A118, which is attributed to the number of calibrated GRBs in A220 (79 GRBs) and this is apparently larger than the one in A118 (20 GRBs). Furthermore, the value of the 1σ uncertainty of the slope b in the A220 and A118 data sets is smaller than that obtained in Liu et al. (2022b)($b = 1.290^{+0.126}_{-0.126}$ in A220, and $b = 0.99^{+0.205}_{-0.205}$ in A118, respectively), by the linear interpolation from SNe Ia with setting $M = -19.36$ as a constant. The intrinsic scatter $\sigma_{\rm int}$ from the A118 GRB data set is smaller than the one from the A220 GRB data set. This character agrees with the results obtained in Khadka et al. (2021), which indicate that the A118 data set is a higher-quality one compared to the A220 data set.

Table 1. Calibration Results (a and b) of the Amati Relation at $z < 1.4$ and the absolute magnitude M of the Pantheon sample fitted by *emcee* with A220 and A118 GRB Data Sets with the 1σ Uncertainty.

Data Sets	a	b	$\sigma_{\rm int}$	M
A220 (79 GRBs)	$52.77^{+0.58}_{-0.58}$	$1.298^{+0.090}_{-0.080}$	$0.521^{+0.027}_{-0.034}$	$-19.50^{+1.40}_{-1.40}$
A118 (20 GRBs)	$52.93^{+0.58}_{-0.58}$	$1.01^{+0.14}_{-0.14}$	$0.466^{+0.046}_{-0.063}$	$-19.50^{+1.40}_{-1.40}$

[7] In the calibration procedure, it is inappropriate to directly use the distance moduli of SNe Ia samples since the absolute magnitude M is unknown.

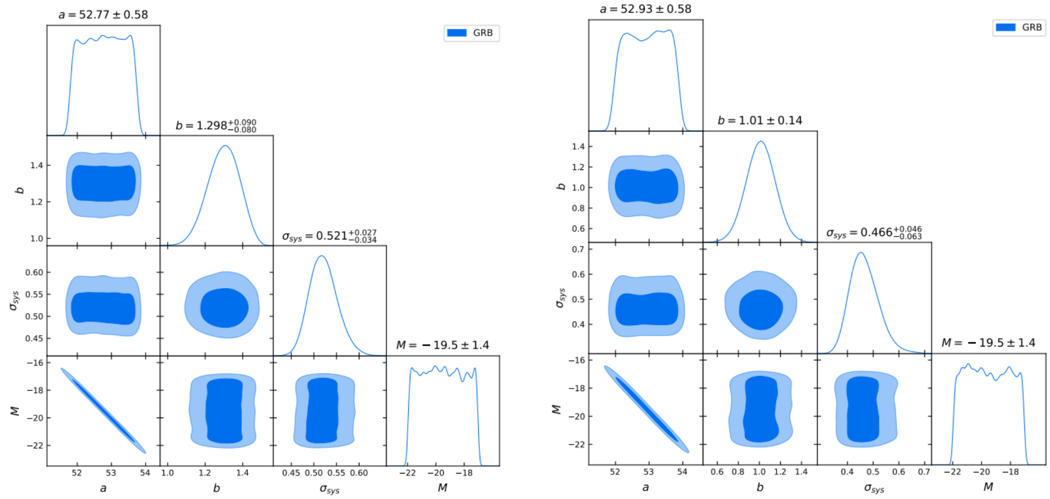

Figure 2. Calibration results (a and b) of the Amati relation at $z < 1.4$ and the absolute magnitude M of the Pantheon sample fitted by *emcee* with GRB data A220 (left panel) and A118 (right panel), respectively.

2.2. *GRB Hubble diagram*

Extrapolating the results from the low-redshift GRBs to the high-redshift ones, we are able to obtain the energy ($E_{\rm iso}$) of each burst at high redshift ($z > 1.4$). Therefore, the luminosity distance (d_L) can be derived. Then, we obtain the GRB Hubble diagram with the A219 sample[8] and A118 sample, which are plotted in Figure 3. The derived distance moduli of 140 GRBs (A219) and 98 GRBs (A118) at $1.4 < z \leq 8.2$ are listed in the Appendix.

The uncertainty of the GRB distance modulus with the Amati relation is

$$\sigma_\mu^2 = \left(\frac{5}{2}\sigma_{\log\frac{E_{\rm iso}}{1{\rm erg}}}\right)^2 + \left(\frac{5}{2{\rm ln}10}\frac{\sigma_{S_{\rm bolo}}}{S_{\rm bolo}}\right)^2, \tag{5}$$

where

$$\sigma^2_{\log\frac{E_{\rm iso}}{1{\rm erg}}} = \sigma^2_{\rm int} + \left(\frac{b}{{\rm ln}10}\frac{\sigma_{E_{\rm p}}}{E_{\rm p}}\right)^2 + \sum\left(\frac{\partial_y(x;\theta_c)}{\partial\theta_i}\right)^2 C_{ii}\,. \tag{6}$$

Here θ_c={$\sigma_{\rm int}$, a, b}, and C_{ii} means the diagonal element of the covariance matrix of these fitting coefficients.

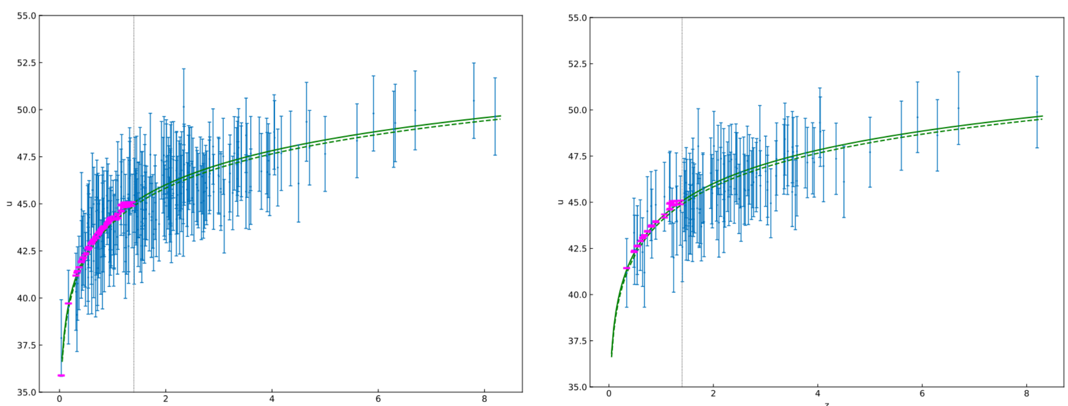

Figure 3. GRB Hubble diagram with the A219 sample (left panel) and the A118 sample (right panel). The GRBs at $z < 1.4$ are obtained by Guassian process from SNe Ia data (purple dots), and the GRBs at $z > 1.4$ (blue dots) are obtained with the Amati relation calibrated with the sample at $z < 1.4$. The solid green curve is the CMB standard distance modulus with H_0 = 67.36 km s^{-1}Mpc^{-1}, $\Omega_{\rm m}$=0.315 (Plank Collaboration 2020), and the green long dotted curve is the SNIa standard distance modulus with H_0 = 74.3 km s^{-1}Mpc^{-1}, $\Omega_{\rm m}$=0.298 (Scolnic et al. 2018). The black dashed line denotes $z = 1.4$.

[8] We remove one point GRB 051109A in the A220 (A102) sample (Khadka et al. 2021) to obtain the A219 sample, in which 140 GRBs at $1.4 < z \leq 8.2$ (see the Appendix for details).

3. CONSTRAINTS ON COSMOLOGICAL MODELS

When using GRB data at $z > 1.4$ to constrain cosmological models, the cosmological parameters can be fitted by using the minimization χ^2 method:

$$\chi^2_{\rm GRB} = \sum_{i=1}^{N_2} \left[\frac{\mu_{\rm obs}(z_i) - \mu_{\rm th}(z_i; p, H_0)}{\sigma_{\mu_i}} \right]^2. \tag{7}$$

Here $N_2 = 140$ or 98 denotes the number of high-redshift GRBs in A219 or A118 data sets, $\mu_{\rm th}$ is the theoretical value of distance modulus calculated from the cosmological model, H_0 is the Hubble constant, p represents the cosmological parameters, and $\mu_{\rm obs}$ is the observational value of distance modulus and its error σ_{μ_i}. Considering a flat space[9], for the wCDM model that has a constant equation of state of dark energy, the theoretical value of the luminosity distance can be obtained from

$$d_{L;\rm th} = \frac{c(1+z)}{H_0} \int_0^z \frac{dz}{[\Omega_{\rm m}(1+z)^3 + \Omega_\Lambda(1+z)^{3(1+w)}]^{\frac{1}{2}}}. \tag{8}$$

Here c is the speed of light, and $\Omega_{\rm m}$ and Ω_Λ are the present dimensionless density parameters of matter and dark energy, respectively, which satisfy $\Omega_{\rm m} + \Omega_\Lambda = 1$. For the flat ΛCDM model, $w = -1$.

Except for the GRB data, we also include the OHD to constrain cosmological models. The OHD can be obtained from the galactic age differential method (Jimenez & Loeb 2002), which has advantages to constrain cosmological parameters and distinguish dark energy models. The 31 Hubble parameter measurements at $0.07 < z < 1.965$ (Stern et al. 2010; Moresco et al. 2012; Moresco 2015; Moresco et al. 2016; Zhang et al. 2014; Ratsimbazafy et al. 2017) are used in our analysis. For the OHD data set, the χ^2 has the form

$$\chi^2_{\rm OHD} = \sum_{i=1}^{N_3} \left[\frac{H_{\rm obs}(z_i) - H_{\rm th}(z_i; p, H_0)}{\sigma_{H_i}} \right]^2. \tag{9}$$

Here $N_3 = 31$ denotes the number of the Hubble parameter measurements. Thus, the total χ^2 of GRB and OHD data is

$$\chi^2_{\rm total} = \chi^2_{\rm GRB} + \chi^2_{\rm OHD}. \tag{10}$$

We use the python package `emcee` (Foreman-Mackey et al. 2013) to constrain cosmological models. In each *emcee* procedure we generate 8000 datasets. The results only with 140 GRBs (A219) and 98 GRBs (A118) are shown in Figure 4 (ΛCDM model) and Figure 5 (wCDM model); and the joint results from 140 GRBs (A219) and 98 GRBs (A118) combined with 31 OHD are shown in Figure 6 (ΛCDM model) and Figure 7 (wCDM model). The constraints of Figure 4-7 with the 1σ confidence level are summarized in Table 2[10]. With 98 GRBs at $1.4 < z < 8.2$ in the A118 sample, we obtained $\Omega_{\rm m} = 0.51^{+0.11}_{-0.17}$ for the flat ΛCDM model, and $\Omega_{\rm m} = 0.47^{+0.21}_{-0.17}$, $w = -0.98^{+0.75}_{-0.48}$ for the flat wCDM model. Combining 98 GRBs in the A118 sample with 31 OHD, we obtained $\Omega_{\rm m} = 0.346^{+0.048}_{-0.069}$ and $h = 0.677^{+0.029}_{-0.029}$ for the flat ΛCDM model, and $\Omega_{\rm m} = 0.314^{+0.072}_{-0.055}$, $h = 0.705^{+0.055}_{-0.069}$, $w = -1.23^{+0.33}_{-0.64}$ for the flat wCDM model. Here $h \equiv \frac{H_0}{100{\rm km/s/Mpc}}$. It should be noted that the ΛCDM model ($w = -1$) is consistent within 1σ with 98 GRBs at $1.4 < z < 8.2$ in A118 sample and 31 OHD data sets for the flat wCDM model. Our results are more stringent than the previous analyses ($\Omega_{\rm m} = 0.34^{+0.13}_{-0.15}$, $w = -0.86^{+0.36}_{-0.38}$ at the 2σ confidence level), which made use of 193 GRBs combined with the SNe Ia (Amati et al. 2019). Here we must point out that only the ΛCDM and wCDM models are considered in our discussions since these two models have less model parameters. However, the dark energy models with the redshift-evolving equation of state appear crucial because several scenarios of them are intriguing in order to heal the H_0 tension[11]. We will go further with the evolving dark energy models in future work and we would expect higher error bars on parameters that predict possible dark energy evolution.

We find that the H_0 value from GRBs at high redshift and OHD ($h = 0.677^{+0.029}_{-0.029}$) seem to be favor to the one from the Planck cosmic microwave backgroud (CMB) observations, which is consistent with previous analyses (Liu et al.

[9] The cosmological models have been usually constrained with flat spatial curvature; however, recently works constrain nonspatially flat models with GRBs and results are promising (see, e.g. Khadka et al. (2021); Cao et al. (2022a); Luongo & Muccino (2022)).

[10] GRB data alone are unable to constrain H_0 because of the degeneracy between H_0 and the correlation intercept parameter; therefore H_0 is set to be 70 km s^{-1}Mpc^{-1} for GRB-only analyses in previous works (Khadka et al. 2021; Cao et al. 2022a). In order to compare with the previous analyses, we also set H_0=70 km s^{-1}Mpc^{-1} for the cases only with GRBs. For a free H_0 in the fitting procedure, `emcee` will provide the similar numerical outcome of the $\Omega_{\rm m}$ value, and H_0 is a bound parameter if the absolute magnitude M of SNe Ia is set as a concrete value in the low-redshift calibration.

[11] The constraint on the Hubble constant H_0 can be given with very high-redshift CMB data based on the ΛCDM model ($H_0 = 67.36 \pm 0.54$ km s^{-1}Mpc^{-1}) (Plank Collaboration 2020), which has a more than 4σ deviation from the value of obtained directly from the very low-redshift SNe Ia data ($H_0 = 74.3 \pm 1.42$ km s^{-1}Mpc^{-1}) (Riess et al. 2018). The H_0 tension seems to suggest that there are potentially unknown systematic errors in observational data, or ΛCDM model used to determine the Hubble constant may be inconsistent with the present universe. Observational data at the redshift region ($2 < z < 1000$) are necessary to precisely identify the possible origin of H_0 tension.

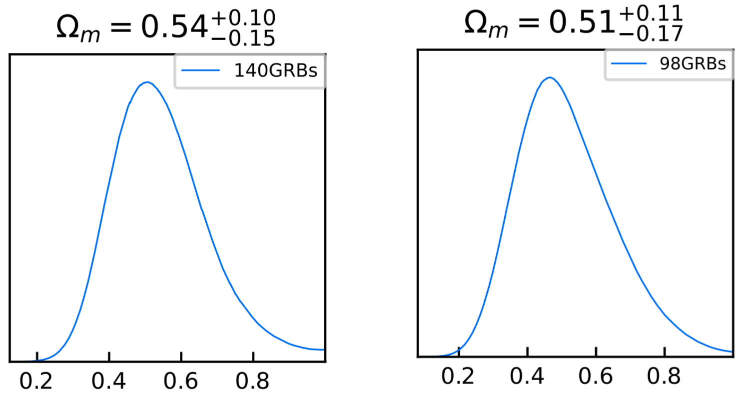

Figure 4. Constraints on Ω_m in the ΛCDM model at high redshift $z > 1.4$ only with 140 GRBs (left panel), and 98 GRBs (right panel). H_0 is set to be 70 km s^{-1}Mpc^{-1}.

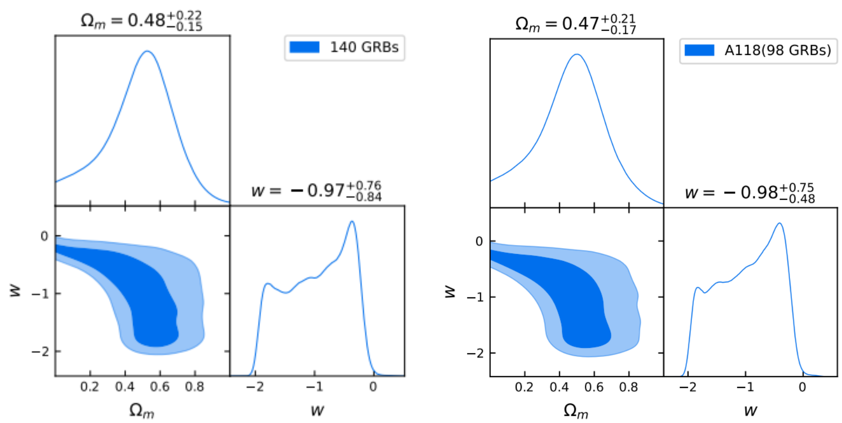

Figure 5. Constraints on Ω_m and w in the wCDM model at high redshift $z > 1.4$ only with 140 GRBs (left panel), and 98 GRBs (right panel). H_0 is set to be 70 km s^{-1}Mpc^{-1}.

Table 2. Constraints on the ΛCDM and wCDM Models at the 1σ Confidence Level from GRBs at high redshift $z > 1.4$, A219 ($z > 1.4$) + 31 OHD, and A118 ($z > 1.4$) + 31 OHD Data Sets.

Models	Data Sets	Ω_m	h	w
	A219 (140 GRBs)	$0.54^{+0.10}_{-0.15}$	-	-
ΛCDM	A118 (98 GRBs)	$0.51^{+0.11}_{-0.17}$	-	-
	A219 (140 GRBs) + 31 OHD	$0.351^{+0.050}_{-0.067}$	$0.677^{+0.029}_{-0.029}$	-
	A118 (98 GRBs) + 31 OHD	$0.346^{+0.048}_{-0.069}$	$0.677^{+0.029}_{-0.029}$	-
	A219 (140 GRBs)	$0.48^{+0.22}_{-0.15}$	-	$-0.97^{+0.76}_{-0.84}$
wCDM	A118 (98 GRBs)	$0.47^{+0.21}_{-0.17}$	-	$-0.98^{+0.75}_{-0.48}$
	A219 (140 GRBs) + 31 OHD	$0.336^{+0.048}_{-0.070}$	$0.710^{+0.055}_{-0.064}$	$-1.30^{+0.30}_{-0.59}$
	A118 (98 GRBs) + 31 OHD	$0.314^{+0.072}_{-0.055}$	$0.705^{+0.055}_{-0.069}$	$-1.23^{+0.33}_{-0.64}$

NOTE—For the cases only with GRBs, h is set to be 0.7.

2022b). We also find the Ω_m value of our results for the flat ΛCDM model with GRBs at high redshift and OHD ($\Omega_\mathrm{m} = 0.346^{+0.048}_{-0.069}$) is consistent with the one from the Planck CMB observations ($\Omega_\mathrm{m} = 0.3153 \pm 0.00073$)(Plank Collaboration 2020) at the 1σ confidence level. Our result of the H_0 value for the flat ΛCDM model appears very well confirmed, while much less for the flat wCDM, which indicate that the H_0 tension instead still persists.

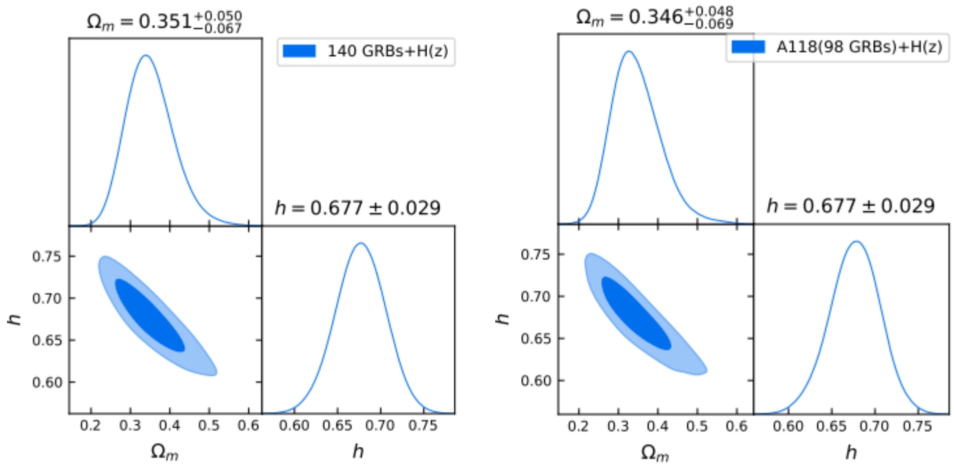

Figure 6. Joint constraints on parameters of Ω_m and h in the ΛCDM model at high redshift $z > 1.4$ with 140 GRBs + 31 OHD (left panel), and 98 GRBs + 31 OHD (right panel).

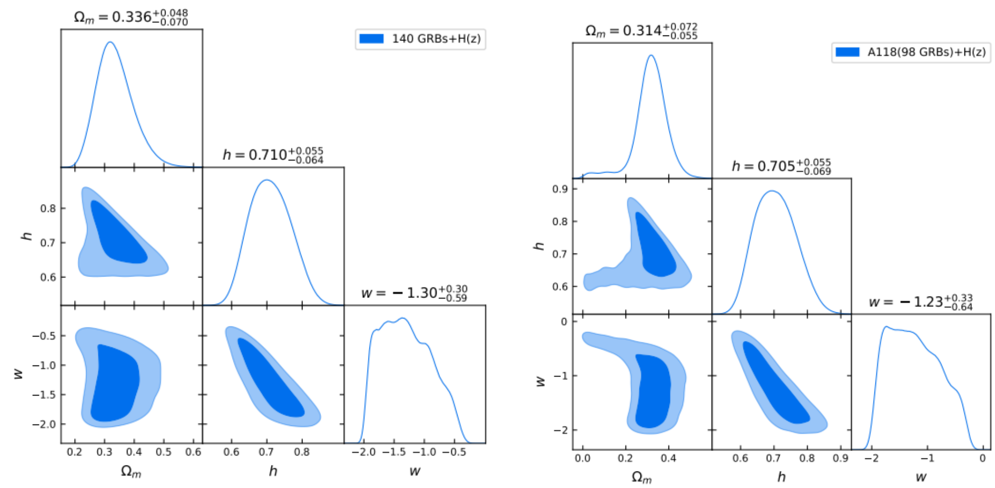

Figure 7. Joint constraints on parameters of $\Omega_{\rm m}$, h and w in the wCDM model at high redshift $z > 1.4$ with 140 GRBs + 31 OHD (left panel), and 98 GRBs + 31 OHD (right panel).

Finally, we also use the A219 and A118 data set to constrain the ΛCDM and wCDM models by using the method of simultaneous fitting. In this calculation, the parameters of cosmological models ($\Omega_{\rm m}$, h, and w) and the relation parameters (a and b) are fitted simultaneously. The number of points that have been used in each *emcee* procedure is 8000. The results from the A219 and A118 samples combined with the OHD data set are shown in Figure 8 (ΛCDM model) and Figure 9 (wCDM model), and summarized in Table 3 with the 1σ confidence level. With the A118 sample and 31 OHD, we obtained $\Omega_{\rm m} = 0.341^{+0.050}_{-0.070}$, $h = 0.673^{+0.029}_{-0.029}$, $a = 52.984^{+0.049}_{-0.049}$, $b = 1.189^{+0.084}_{-0.084}$ for the flat ΛCDM model, and $\Omega_{\rm m} = 0.325^{+0.052}_{-0.064}$, $h = 0.702^{+0.048}_{-0.065}$, $w = -1.25^{+0.51}_{-0.40}$, $a = 52.980^{+0.049}_{-0.049}$, $b = 1.185^{+0.084}_{-0.084}$ for the flat wCDM model. It is found that the values of the coefficients of the Amati relation for the flat ΛCDM model and the flat wCDM model are almost identical, which are consistent with the results calibrating from the low-redshift data at the 1σ confidence level. The values of the 1σ uncertainty of the relation parameters (a, b) and the intrinsic scatter $\sigma_{\rm int}$ in simultaneous fitting are smaller than those listed in Table 1, which is attributed to the number of calibrated GRBs in the A220 or A118 data set, these are apparently larger than those of the 79 GRBs in the A220 sample and 20 GRBs in the A118 sample at $z < 1.4$. We also find that the simultaneous fitting results from only GRBs are consistent with previous analyses (Liu et al. 2022a).[12]

[12] Our simultaneous fitting results with the A219 sample and the A118 sample are slightly different from those with the A220 sample and A118 sample obtained in Khadka et al. (2021) and Cao et al. (2022b). It should be pointed out that there is an error in the peak energy of GRB 081121 data released in Fana Dirirsa et al. (2019) that corresponds to the distance modulus (47.23 ± 1.08) rather than the peak energy (871 ± 1.23) in Table 4 of Wang et al. (2016). Therefore, we correct this error in our work.

Table 3. Simultaneous Fitting Results of $\Omega_{\rm m}$, h, a, b and $\sigma_{\rm int}$ in the ΛCDM and wCDM Models, with A219 GRB + 31 OHD, and A118 GRB + 31 OHD Data Sets.

Models	Data Sets	Ω_m	h	w	a	b	$\sigma_{\rm int}$
ΛCDM	A219 GRB + 31 OHD	$0.378^{+0.053}_{-0.074}$	$0.659^{+0.029}_{-0.029}$	-	$52.841^{+0.039}_{-0.039}$	$1.327^{+0.073}_{-0.073}$	$0.465^{+0.022}_{-0.025}$
	A118 GRB + 31 OHD	$0.341^{+0.050}_{-0.070}$	$0.673^{+0.029}_{-0.029}$	-	$52.984^{+0.049}_{-0.049}$	$1.189^{+0.084}_{-0.084}$	$0.392^{+0.024}_{-0.030}$
wCDM	A219 GRB + 31 OHD	$0.351^{+0.074}_{-0.067}$	$0.672^{+0.047}_{-0.064}$	$-1.14^{+0.45}_{-0.45}$	$52.842^{+0.039}_{-0.039}$	$1.330^{+0.074}_{-0.074}$	$0.463^{+0.022}_{-0.026}$
	A118 GRB + 31 OHD	$0.325^{+0.052}_{-0.064}$	$0.702^{+0.048}_{-0.065}$	$-1.25^{+0.51}_{-0.40}$	$52.980^{+0.049}_{-0.049}$	$1.185^{+0.084}_{-0.084}$	$0.392^{+0.025}_{-0.031}$

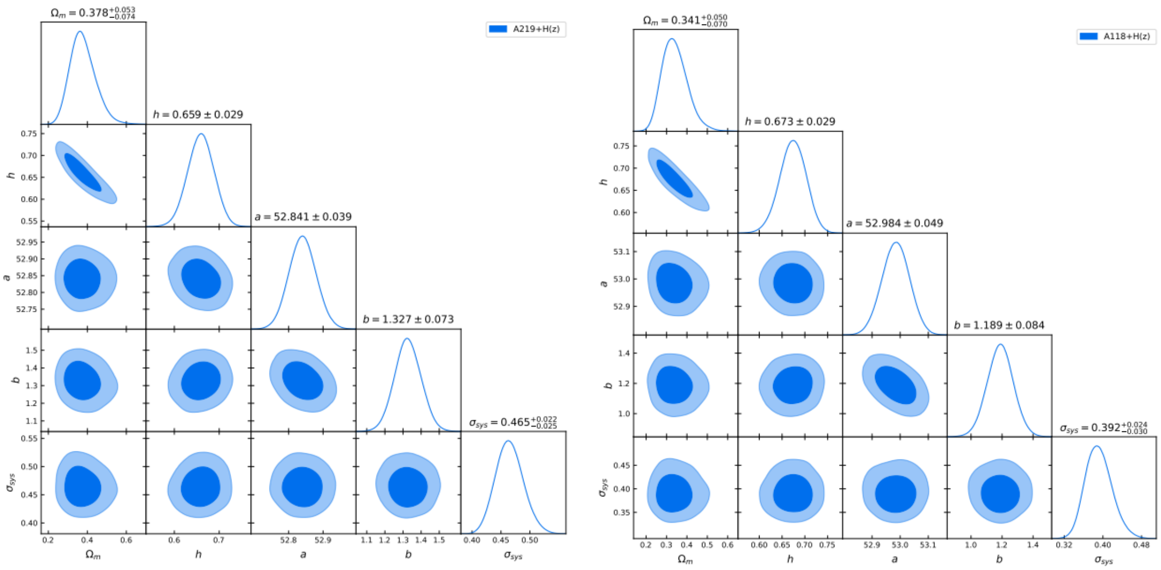

Figure 8. Simultaneous fitting parameters of Ω_m, h, a, b and σ_{int} in the ΛCDM model with A219 GRBs + 31 OHD (left panel), and A118 GRBs + 31 OHD (right panel).

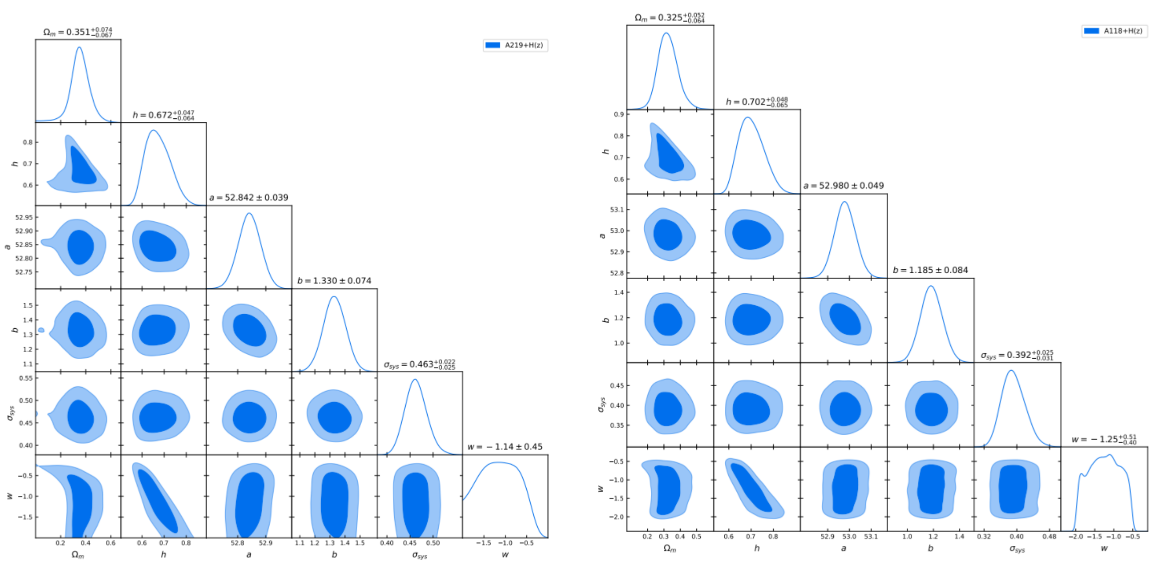

Figure 9. Simultaneous fitting parameters of Ω_m, h, a, b, σ_{int} and w in the wCDM model with A219 GRBs + 31 OHD (left panel), and A118 GRBs + 31 OHD (right panel).

4. CONCLUSIONS AND DISCUSSIONS

In this paper, we use the Gaussian process to calibrate the Amati relation of GRB from SNe Ia data and obtain the GRB Hubble diagram with GRB data sets of the A219 and A118 samples. Then, these GRB data are used to constrain the ΛCDM and wCDM models. With 98 GRBs at $1.4 < z \leq 8.2$ in the A118 sample, we obtained $\Omega_{\rm m} = 0.51^{+0.11}_{-0.17}$ for the flat ΛCDM model, and $\Omega_{\rm m} = 0.47^{+0.21}_{-0.17}$, $w = -0.98^{+0.75}_{-0.48}$ for the flat wCDM model at the 1σ confidence level. With 98 GRBs at $1.4 < z < 8.2$ in the A118 sample and 31 OHD, we obtained $\Omega_{\rm m} = 0.346^{+0.048}_{-0.069}$ and $h = 0.677^{+0.029}_{-0.029}$ for the flat ΛCDM model, and $\Omega_{\rm m} = 0.314^{+0.072}_{-0.055}$, $h = 0.705^{+0.055}_{-0.069}$, $w = -1.23^{+0.33}_{-0.64}$ for the flat wCDM model at the 1σ confidence level. With GRBs at high redshift and OHD date sets, we find that the H_0 value seems to favor the one from the Planck CMB observations, and the $\Omega_{\rm m}$ value of our results for the flat ΛCDM model is consistent with the one from the Planck CMB observations at the 1σ confidence level. We also use GRB data sets of A219 and A118 samples to fit $\Omega_{\rm m}$, h, a, b, $\sigma_{\rm int}$ and w parameters simultaneously. It is found that the simultaneous fitting results are consistent with those obtained from the low-redshift calibration method.

Furthermore, there are some discussions on possible evolutionary effects in GRB relations (Li 2007; Basilakos & Perivolaropoulos 2008; Ghirlanda et al. 2008; Tsutsui et al. 2009b; Wang et al. 2011). Recently, Lin et al. (2016) investigated the six relations in two redshift bins, and found moderate evidence for the redshift evolution in four relations. Demianski et al. (2017a) found no redshift evolution in the Amati relation with 162 GRB samples. Wang et al. (2017) found the Amati relation evolves with redshift. More recently, Khadka et al. (2021) found that the Amati relation is independent of redshift within the error bars with the A220 GRB data set. Dai et al. (2021) found strong evidence that the Amati relation shows no, or marginal, evolution with redshift. Tang et al. (2021) found that the intercept and slope of the Amati relation for the low-z subsample and high-z subsample differ at more than 2σ. As a result, whether the GRB relations are redshift dependent or not is still under debate. Nevertheless, further examinations of possible evolutionary effects should be required for considering GRBs as standard candles for a cosmological probe.

ACKNOWLEDGMENTS

We thank Prof. Pan Yu, Prof. Feng Jianchao, Prof. Peng Junjin, and Yang Liu, Zhang Bin, Xie Hanbei for kind help and discussions. We also thank the referee for helpful comments and constructive suggestions. This project was supported by the Guizhou Provincail Science and Technology Foundation (QKHJC-ZK[2021] Key 020), in part by the NSFC under Grants Nos. 12275080, 12075084, 11690034, 11805063, and 12073069, and by the Science and Technology Innovation Plan of Hunan province under Grant No. 2017XK2019.

APPENDIX

REFERENCES

Amati, L., D'Agostino, R., Luongo, O., Muccino, M., & Tantalo, M. 2019, MNRAS, 486, L46

Amati, L., Frontera, F., Tavani, M., et al. 2002, A&A, 390, 81

Amati, L., Guidorzi, C., Frontera, F., et al. 2008, MNRAS, 391, 577

Avila, F., Bernui, A., Nunes, R. C., et al. 2022, MNRAS, 509, 2294

Aviles, A., Gruber, C., Luongo, O., & Quevedo, H. 2012, PhRvD, 86, 123516

Basilakos, S., & Perivolaropoulos, L. 2008, MNRAS, 391, 411

Busti, V. C., Clarkson, C., & Seikel, M. 2014, MNRAS, 441, L11

Cao, S., Dainotti, M., & Ratra, B. 2022a, MNRAS, 512, 439

Cao, S., Khadka, N., & Ratra, B. 2022b, MNRAS, 510, 2928

Cao, S., & Ratra, B.

Cao, S., Ryan, J., Khadka, N., & Ratra, B. 2021, MNRAS, 501, 1520

2022, MNRAS, 513, 5686

Capozziello, S., & Izzo, L. 2008, A&A, 490, 31

Capozziello, S. & Izzo, L. 2009, NuPhS, 194, 206

Capozziello, S., & Izzo, L. 2010, A&A, 519, A73

Capozziello, S., D'Agostino, R., & Luongo, O. 2018, MNRAS, 476, 3924

Table 4. List of the derived distance moduli of 140 GRBs in the A219 sample at $1.4 < z \leq 8.2$.

GRB	z	$\mu_{\rm GRB} \pm \sigma_{\mu,\rm GRB}$	GRB	z	$\mu_{\rm GRB} \pm \sigma_{\mu,\rm GRB}$	GRB	z	$\mu_{\rm GRB} \pm \sigma_{\mu,\rm GRB}$
120711A	1.405	45.44 ± 1.96	070521	2.0865	45.87 ± 1.95	050401	2.9	45.63 ± 1.99
160625B	1.406	42.69 ± 1.95	150206A	2.087	44.93 ± 1.96	141109A	2.993	46.52 ± 2.00
151029A	1.423	46.53 ± 1.99	061222A	2.088	45.95 ± 1.97	090715B	3	46.45 ± 2.00
050318	1.44	44.78 ± 1.97	130610	2.09	47.23 ± 1.96	080607	3.036	45.80 ± 1.96
100814	1.44	44.89 ± 1.96	100728B	2.106	47.38 ± 1.95	081028	3.038	45.62 ± 2.03
141221A	1.452	46.61 ± 1.97	090926A	2.1062	43.82 ± 1.95	060607A	3.082	47.52 ± 2.01
110213	1.46	44.31 ± 2.00	011211	2.14	45.55 ± 1.96	120922	3.1	44.34 ± 1.95
010222	1.48	43.62 ± 1.95	071020	2.145	47.34 ± 2.02	020124	3.2	46.15 ± 2.00
120724	1.48	45.19 ± 1.99	050922C	2.198	46.76 ± 2.01	060526	3.21	46.61 ± 2.04
060418	1.489	45.22 ± 1.99	120624B	2.2	44.18 ± 1.95	140423A	3.26	45.57 ± 1.95
150301B	1.5169	47.09 ± 1.95	121128	2.2	45.34 ± 1.95	140808A	3.29	47.67 ± 1.95
030328	1.52	43.34 ± 1.96	080804	2.2045	46.89 ± 1.95	160629A	3.332	47.08 ± 1.95
070125	1.547	44.03 ± 1.96	110205	2.22	45.47 ± 2.05	080810	3.35	47.41 ± 1.96
090102	1.547	45.78 ± 1.97	180325A	2.248	46.36 ± 1.97	061222B	3.355	46.32 ± 1.97
161117A	1.549	42.76 ± 1.95	081221	2.26	44.27 ± 1.94	110818	3.36	47.62 ± 1.97
060306	1.559	45.72 ± 2.05	130505	2.27	46.58 ± 1.95	030323	3.37	47.98 ± 2.06
040912	1.563	44.24 ± 2.24	140629A	2.275	46.19 ± 1.99	971214	3.42	47.15 ± 1.97
100728A	1.567	43.95 ± 1.95	060124	2.296	45.55 ± 2.02	060707	3.425	47.33 ± 1.96
990123	1.6	43.84 ± 1.99	021004	2.3	46.77 ± 2.05	170405A	3.51	45.64 ± 1.95
071003	1.604	46.18 ± 1.96	141028A	2.33	45.90 ± 1.95	110721A	3.512	48.63 ± 1.97
090418	1.608	46.67 ± 2.00	151021A	2.33	44.18 ± 1.96	060115	3.53	47.30 ± 1.96
110503	1.61	45.07 ± 1.95	110128A	2.339	50.15 ± 2.01	090323	3.57	45.60 ± 1.95
990510	1.619	44.72 ± 1.96	051109A	2.346	47.09 ± 2.02	100704	3.6	47.67 ± 1.96
080605	1.6398	45.04 ± 1.95	131108A	2.4	45.75 ± 1.95	130514	3.6	45.91 ± 2.00
131105A	1.69	44.46 ± 1.96	171222A	2.409	45.22 ± 1.95	130408	3.76	47.63 ± 1.97
091020	1.71	47.61 ± 2.19	060908	2.43	46.66 ± 1.97	120802	3.8	46.72 ± 2.01
100906	1.73	44.30 ± 2.14	080413	2.433	47.13 ± 2.01	100413	3.9	47.53 ± 2.00
120119	1.73	44.12 ± 1.96	090812	2.452	47.02 ± 2.02	060210	3.91	46.68 ± 2.10
150314A	1.758	44.59 ± 1.95	120716A	2.486	47.12 ± 1.95	120909	3.93	47.29 ± 1.95
110422	1.77	43.39 ± 1.94	130518A	2.49	45.30 ± 1.95	140419A	3.956	46.56 ± 2.19
080514B	1.8	45.61 ± 1.97	081121	2.512	46.51 ± 1.97	131117A	4.04	48.81 ± 1.97
120326	1.8	45.06 ± 1.95	170214A	2.53	44.97 ± 1.95	060206	4.048	48.50 ± 1.96
090902B	1.822	44.15 ± 1.95	081118	2.58	46.03 ± 1.96	090516	4.109	46.92 ± 2.04
131011A	1.874	43.92 ± 1.96	080721	2.591	45.85 ± 1.97	120712A	4.1745	47.68 ± 1.97
140623A	1.92	47.31 ± 2.05	050820	2.612	45.70 ± 1.97	080916C	4.35	47.93 ± 1.98
080319C	1.95	46.52 ± 2.00	030429	2.65	46.57 ± 1.97	000131	4.5	46.07 ± 2.04
170113A	1.968	47.57 ± 2.06	120811C	2.67	45.06 ± 1.96	090205	4.6497	49.35 ± 2.09
081008	1.9685	45.25 ± 1.97	080603B	2.69	46.45 ± 1.98	140518A	4.707	47.97 ± 1.97
030226	1.98	45.07 ± 1.97	161023A	2.708	45.15 ± 1.98	111008	5	47.65 ± 1.99
130612	2.01	47.49 ± 1.96	060714	2.711	45.60 ± 2.08	060927	5.6	48.34 ± 1.96
170705A	2.01	44.88 ± 1.95	140206A	2.73	45.65 ± 1.95	130606	5.91	49.79 ± 1.99
161017A	2.013	47.27 ± 1.96	091029	2.752	46.11 ± 1.99	050904	6.29	48.96 ± 2.02
140620A	2.04	45.61 ± 1.95	081222	2.77	45.84 ± 1.95	140515A	6.32	49.29 ± 2.05
081203A	2.05	46.41 ± 2.11	050603	2.821	46.42 ± 1.95	080913	6.695	49.96 ± 2.09
150403A	2.06	46.12 ± 1.95	161014A	2.823	47.38 ± 1.95	120923A	7.8	50.47 ± 2.00
000926	2.07	44.45 ± 1.96	110731	2.83	46.60 ± 1.95	090423	8.2	49.63 ± 2.05
080207	2.0858	45.55 ± 2.18	111107	2.89	48.04 ± 2.00			

Note—For the A220 sample (Khadka et al. 2021), there are two distance moduli of GRB051109A at $z = 2.346$ calculated by different peak energy and bolometric fluence. In Table 7 of Khadka et al. (2021) for the A118 sample, $E_{\rm p}$=539 ± 200, $S_{\rm bolo}$=0.51 ± 0.05; while in Table 8 of Khadka et al. (2021) for the A102 (A220) sample, which are compiled from those listed in Demianski et al. (2017a), $E_{\rm p}$=538.706 ± 274.372, $S_{\rm bolo}$=0.519357 ± 0.269718. However, we find that $E_{\rm p}$=539 ± 200, $E_{\rm iso}$=6.84516 ± 0.730151 in Table 5 of Demianski et al. (2017a), and $E_{\rm p}$=539 ± 200, $S_{\rm bolo}$=0.51 ± 0.05 in Table 1 of Amati et al. (2008). We remove GRB051109A in A102 (A220) sample, therefore we obtain 140 GRBs at $1.4 < z \leq 8.2$ in the A219 sample.

Table 5. List of the derived distance moduli of 98 GRBs in the A118 sample at $1.4 < z \leq 8.2$.

GRB	z	$\mu_{\rm GRB} \pm \sigma_{\mu,\rm GRB}$	GRB	z	$\mu_{\rm GRB} \pm \sigma_{\mu,\rm GRB}$	GRB	z	$\mu_{\rm GRB} \pm \sigma_{\mu,\rm GRB}$
160625B	1.406	42.57 ± 1.87	130610	2.09	47.28 ± 1.87	090715B	3	46.67 ± 1.90
050318	1.44	45.48 ± 1.88	090926A	2.1062	43.89 ± 1.86	080607	3.036	45.66 ± 1.88
100814	1.44	45.28 ± 1.87	011211	2.14	46.10 ± 1.87	081028	3.038	46.10 ± 1.91
110213	1.46	44.81 ± 1.89	071020	2.145	47.35 ± 1.94	120922	3.1	44.94 ± 1.86
010222	1.48	43.73 ± 1.86	050922C	2.198	47.06 ± 1.91	020124	3.2	46.43 ± 1.89
120724	1.48	46.05 ± 1.90	120624B	2.2	44.14 ± 1.87	060526	3.21	47.34 ± 1.95
060418	1.489	45.42 ± 1.89	121128	2.2	45.81 ± 1.86	080810	3.35	47.31 ± 1.88
030328	1.52	43.71 ± 1.87	110205	2.22	45.58 ± 1.93	110818	3.36	47.61 ± 1.88
070125	1.547	44.08 ± 1.87	130505	2.27	46.38 ± 1.88	030323	3.37	48.41 ± 1.94
090102	1.547	45.76 ± 1.88	060124	2.296	45.64 ± 1.91	971214	3.42	47.30 ± 1.88
040912	1.563	45.24 ± 2.07	021004	2.3	47.21 ± 1.92	060707	3.425	47.76 ± 1.87
100728A	1.567	44.05 ± 1.86	141028A	2.33	45.83 ± 1.87	170405A	3.51	45.55 ± 1.87
990123	1.6	43.70 ± 1.91	051109A	2.346	47.31 ± 1.90	110721A	3.512	47.98 ± 1.93
071003	1.604	45.97 ± 1.89	131108A	2.4	45.73 ± 1.87	060115	3.53	47.71 ± 1.87
090418	1.608	46.55 ± 1.91	060908	2.43	46.90 ± 1.87	090323	3.57	45.39 ± 1.88
110503	1.61	45.27 ± 1.86	080413	2.433	47.32 ± 1.91	100704	3.6	47.76 ± 1.87
990510	1.619	45.01 ± 1.87	090812	2.452	46.83 ± 1.93	130514	3.6	46.15 ± 1.89
080605	1.6398	45.20 ± 1.86	130518A	2.49	45.18 ± 1.87	130408	3.76	47.65 ± 1.88
131105A	1.69	44.67 ± 1.87	081121	2.512	46.58 ± 1.88	120802	3.8	47.15 ± 1.90
091020	1.71	48.03 ± 2.03	170214A	2.53	44.76 ± 1.88	100413	3.9	47.37 ± 1.92
100906	1.73	44.62 ± 1.99	081118	2.58	46.65 ± 1.88	120909	3.93	47.15 ± 1.88
120119	1.73	44.42 ± 1.87	080721	2.591	45.70 ± 1.89	131117A	4.04	49.30 ± 1.88
150314A	1.758	44.62 ± 1.86	050820	2.612	45.63 ± 1.88	060206	4.048	48.82 ± 1.87
110422	1.77	43.68 ± 1.86	030429	2.65	47.23 ± 1.88	090516	4.109	46.95 ± 1.93
080514B	1.8	45.78 ± 1.88	120811C	2.67	45.66 ± 1.87	080916C	4.35	47.35 ± 1.92
120326	1.8	45.72 ± 1.86	080603B	2.69	46.77 ± 1.88	000131	4.5	46.10 ± 1.93
090902B	1.822	43.93 ± 1.88	140206A	2.73	45.92 ± 1.86	111008	5	47.70 ± 1.89
080319C	1.95	46.57 ± 1.90	091029	2.752	46.59 ± 1.88	060927	5.6	48.60 ± 1.87
081008	1.9685	45.70 ± 1.87	081222	2.77	46.08 ± 1.86	130606	5.91	49.60 ± 1.91
030226	1.98	45.48 ± 1.87	050603	2.821	46.36 ± 1.87	050904	6.29	48.62 ± 1.93
130612	2.01	48.04 ± 1.87	110731	2.83	46.57 ± 1.87	080913	6.695	50.09 ± 1.96
150403A	2.06	45.86 ± 1.88	111107	2.89	48.33 ± 1.89	090423	8.2	49.88 ± 1.93
000926	2.07	44.84 ± 1.87	050401	2.9	45.89 ± 1.89			

Cardone, V. F., Capozziello, S., & Dainotti, M. G., 2009, MNRAS, 400, 775
Cardone, V. F., Perillo, M. & Capozziello, S., 2011, MNRAS, 417, 1672
Cucchiara, A., Levan, A., Fox, D. B., et al. 2011, ApJ, 736, 7
D'Agostini, G. 2005, arXiv: physics/0511182
Dai, Y., Zheng, X.-G., Li, Z. X., Gao, H. & Zhu Z.-H. 2021, A&A, 651, L8
Dai, Z., Liang, E., & Xu, D. 2004, ApJ, 612, L101
Dainotti, M. G., Cardone V. F., & Capozziello S. 2008, MNRAS, 391, L79
Dainotti, M. G., & Del Vecchio, R., 2017, NewAR, 77, 23
Dainotti,M. G., & Amati, L., 2018, PASP, 130, 051001
Dainotti, M. G., Young, S., Li, L., et al. 2022a, ApJS, 261, 25
Dainotti, M. G., Nielson, V., Sarracino, G., et al. 2022b, MNRAS, 514, 1828
Dainotti, M. G., Lenart, A. L., Chraya, A., et al. 2023, MNRAS, 518, 2201 (arXiv:2209.08675)
Demianski, M., & Piedipalumbo, E., 2011, MNRAS, 415, 3580
Demianski, M., Piedipalumbo, E., & Rubano, C. 2011, MNRAS, 411, 1213
Demianski, M., Piedipalumbo, E., Sawant, D., & Amati, L. 2017, A&A, 598, A112
Demianski, M., Piedipalumbo, E., Sawant, D., & Amati, L. 2017, A&A, 598, A113
Demianski, M., Piedipalumbo, E., Sawant, D., & Amati, L. 2021, MNRAS, 506, 903
Dunsby, P. K. S. & Luongo, O. 2016, IJGMM, 13, 03, 1630002
Fana Dirirsa, F., Razzaque, S., Piron, F., et al. 2019, ApJ, 887, 13
Feng, C.-J., & Li, X.-Z. 2016, ApJ, 821, 30
Fenimore, E. E., & Ramirez-Ruiz, E. 2000, arXiv preprint astro-ph/0004176
Firmani, C., Ghisellini, G., Avila-Reese, V., & Ghirlanda, G. 2006, MNRAS, 370, 185
Firmani, C., Ghisellini, G., Ghirlanda, G., & Avila-Reese, V. 2005, MNRAS, 360, L1
Foreman-Mackey, D., Hogg, D. W., Lang, D., & Goodman, J. 2013, PASP, 125, 306
Freitas, R. C., Gonçalves, S. V. B., & Velten, H. E. S. 2011, Phys. Lett. B, 703, 209
Gao, H., Liang, N., & Zhu, Z.-H. 2012, IJMPD, 21, 1250016
Ghirlanda, G., Ghisellini, G., & Lazzati, D. 2004a, ApJ, 616, 331
Ghirlanda, G., Ghisellini, G., Lazzati, D., & Firmani, C. 2004b, ApJ, 613, L13
Ghirlanda, G., Ghisellini, G.,& Firmani, C. 2006, New, J. Phys., 8, 123
Ghirlanda, G., Nava, L., Ghisellini, G., Firmani, C., & Cabrera, J. I. 2008, MNRAS, 387, 319
Gowri G. & Shantanu D. 2022, JCAP, 10, 069
Gruber, C. & Luongo, O. 2014, PhRvD, 89, 103506
Hu, J. P., Wang, F. Y., & Dai, Z. G. 2021, MNRAS, 507, 730
Izzo, L., Capozziello, S., Covone, G., & Capaccioli, M. 2009, A&A, 508, 63
Izzo, L., Muccino, M., Zaninoni, E., Amati, L., & Della Valle, M., 2015, A&A, 582, A115
Jia, X. D., Hu, J. P., Yang, J., Zhang, B. B., & Wang, F. Y. 2022, MNRAS, 516, 2575
Jimenez, R., & Loeb, A. 2002, ApJ, 573, 37
Khadka, N. & Ratra, B. 2020, MNRAS, 499, 391
Khadka, N., Luongo, O., Muccino, M., & Ratra, B. 2021, JCAP, 09, 042
Kodama, Y., Yonetoku, D., Murakami, T., et al. 2008, MNRAS, 391, L1
Li, L. X. 2007, MNRAS, 379, L55
Li, H., Xia, J.-Q., Liu, J., et al. 2008, ApJ, 680, 92
Liang, E., & Zhang, B. 2005, ApJ, 633, 611
Liang, E., & Zhang, B. 2006, MNRAS, 369, L37
Liang, N., Xiao, W. K., Liu, Y., & Zhang, S. N. 2008, ApJ, 685, 354
Liang, N., & Zhang, S. 2008, AIP Conf. Proc. Vol. 1065, Am. Inst. Phys New York
Liang, N., Wu, P., & Zhang, S. N. 2010, PhRvD, 81, 083518
Liang, N., Xu, L., & Zhu, Z. H. 2011, A&A, 527, A11
Lin, H. N., Li, X., Chang, Z. 2016, MNRAS, 455, 2131
Lin, H. N., Li, M. H., & Li, X. 2018, MNRAS, 480, 3117
Liu, J., & Wei, H. 2015, **GReGr**, 47, 141
Liu, Y., Chen, F., Liang, N., et al. 2022, ApJ, 931, 50
Liu, Y., Liang, N., Xie, X., et al. 2022, ApJ, 935, 7
Luongo, O., & Muccino, M. 2020, A&A, 641, A174
Luongo, O., & Muccino, M. 2021, MNRAS, 503, 4581
Luongo, O., & Muccino, M. 2021, Galaxies, 9, 77
Luongo, O., & Muccino, M. 2023, MNRAS, 518, 2247(arXiv:2207.00440)
Montiel, A., Cabrera, J. I., & Hidalgo, J. C. 2021, MNRAS, 467, 3239
Moresco, M. 2015, MNRAS, 450, L16
Moresco, M., Cimatti, A., Jimenez, R., et al. 2012, JCAP, 08, 006
Moresco, M., Pozzetti, L., Cimatti, A. et al. 2016, JCAP, 05, 014
Muccino, M., Izzo, L., Luongo, O., Boshkayev, K., Amati, L., Della Valle, M., Pisani, G. B., & Zaninoni, E. 2021, ApJ, 908, 181

Muccino, M., Luongo, O., & Jain, D., 2022, arXiv: 2208.13700
Norris, J. P., Marani, G. F., & Bonnell, J. T. 2000, ApJ, 534, 248
Pan, Y., Qi, J., Cao, S., et al. 2020, ApJ, 890, 169
Perlmutter, S., Aldering, G., Goldhaber, G., et al. 1999, ApJ, 517, 565
Plank Collaboration. Aghanim, N., Akrami, Y., Arroja, F., et al. 2020, A&A, 641, A1
Ratsimbazafy, A. L., Loubser, S. I., Crawford, S. M., et al. 2017, MNRAS, 467, 3239
Riess, A. G., Filippenko, A. V., Challis, P., et al. 1998, AJ, 116, 1009
Riess, A. G., Casertano, S., Yuan, W., et al. 2018, ApJ, 861, 126
Schaefer, B. E. 2003, ApJ, 583, L67
Schaefer, B. E. 2007, ApJ, 660, 16
Scolnic, D. M., Jones, D. O., Rest, A., et al. 2018, ApJ, 859, 101
Seikel, M., Clarkson, C., & Smith, M. 2012, JCAP, 06, 036
Seikel, M., Yahya, S., Maartens, R., & Clarkson, C. 2012, PhRvD, 86, 083001
Shirokov, S. I., Sokolov, I. V., Lovyagin, N. Yu, et al. 2020, MNRAS, 496, 1530
Stern D., Jimenez R., Verde L., Kamionkowski M., & Stanford S. A. 2010, JCAP, 02, 008
Sun, W., Jiao, K., & Zhang, T.-J. 2021, ApJ, 915, 123
Tang L., Li X., Lin, H.-N., & Liu L. 2021, ApJ, 907, 121
Tang L., Lin, H.-N., Li X., & Liu L. 2022, MNRAS, 509, 1194
Tsutsui, R., Nakamura, T., Yonetoku, D., Murakami, T., Kodama, Y., & Takahashi, K. 2009, JCAP, 0908, 015
Tsutsui, R., Nakamura, T., Yonetoku, D., Murakami, T., Tanabe, S., Kodama, Y. & Takahashi, K. 2009, MNRAS, 394, L31
Wang, Y. 2008, PhRvD, 78, 123532
Wang, F., & Dai, Z. G. 2006, MNRAS, 368, 371
Wang, F. Y., & Dai, Z. G. 2011, A&A, 536, 96
Wang, F. Y., Dai, Z. G., & Liang, E. W. 2015, NewAR, 67, 1
Wang, F. Y., Qi, S., & Dai, Z. G. 2011, MNRAS, 415, 3423
Wang, F. Y., Hu, J. P., Zhang, G. Q., & Dai, Z. G. 2022, ApJ, 924, 97
Wang, J. S., & Wang, F. Y. 2014, MNRAS, 443, 1680
Wang, J. S., Wang, F. Y., Cheng, K. S., & Dai, Z. G. 2016, A&A, 585, A68
Wang, G. J., Yu, H., Li, Z. X., Xia, J. Q., & Zhu Z.-H. 2017, ApJ, 836, 103
Wang, Y. Y., & Wang, F. Y. 2019, ApJ, 873, 39
Wei, H., Zhang, S. N. 2009, EPJC, 63, 139
Wei, H., 2010, JCAP, 08, 020
Wei, J. J., Ma, Q.-B., & Wu, Xue-Feng 2015, Advances in Astronomy Volume 2015, Article ID 576093
Wei, J. J., 2018, ApJ, 868, 29
Xu, D., Dai, Z., & Liang, E. 2005, ApJ, 633, 603
Xu, F., Tang, C.-H., Geng, J.-J., Wang, F.-Y., Wang, Y.-Y., Kuerban, A. & Huang, Y.-F. 2021, ApJ, 920, 135
Yonetoku, D., Murakami, T., Nakamura, T., et al. 2004, ApJ, 609, 935
Yu, B., Qi, S., & Lu, T. **2009**, ApJ, 705, L15
Yu, H., Wang, F. Y. 2016, ApJ, 828, 85
Yu, H., Ratra, B., & Wang, F. Y. 2018, ApJ, 856, 3
Zhang, C., Zhang, H., Yuan, S., et al. 2014, RAA, 14, 1221